

# Flow Visualisation and Particle Dispersion Measurements Inside an Ambulance Rear Saloon whilst Stationary and in Motion

\*Nicholas J. Lawson<sup>1,2</sup>, Kim Blackburn<sup>1</sup>, Glenn Sherwood<sup>1</sup>, James Brighton<sup>1</sup>, Helen V. Atkinson<sup>1</sup>

1. School of Aerospace, Transport Systems and Manufacturing  
Cranfield University, Cranfield, Bedfordshire MK43 0AL, U.K.
2. Now with: School of Aerospace, Mechanical and Mechatronic Engineering, The University of Sydney, Camperdown, NSW 2006, Australia

\*Corresponding author email: [nicholas.lawson@sydney.edu.au](mailto:nicholas.lawson@sydney.edu.au)

Keywords: flow visualisation, particle image velocimetry, particle sizing, in-vehicle flows

## Abstract

The following paper presents flow field and particle dispersion data from a UK National Health Service (NHS) ambulance, under static and dynamic driving conditions and when using different ventilation modes. Data was recorded using laser sheet flow visualisation, particle image velocimetry and hot wire anemometry, from a common plane positioned about the patient centreline. Results indicated a significant influence of the ceiling fan ventilation system on gross flow field behaviour, with the ventilation fan on extract or intake mode. With either ventilation mode, flow velocities in the patient region were found to double from a quiescent condition, to around 50mm/s – 100mm/s. Particle dispersion data also showed dispersion decay rates over five times faster when using the ceiling fan extraction system. All these results were consistent when the vehicle was stationary or driving at a constant speed of 60mph. However, with the vehicle under dynamic driving conditions, such as acceleration or braking, the regular flow patterns were substantially disrupted, with bulk movement of the flow in the direction of the acceleration or braking action. Under these dynamic conditions, the magnitude of the net velocity change on the fluid exceeded any flow generated from the ceiling ventilation system.

## 1. Introduction

Understanding vehicle interior flows is seen as an important part of the vehicle design, to ensure a suitable environment for the driver and occupants [1 - 6]. A number of approaches to characterising the flow field have been reported and focus on basic flow visualisation and computational fluid dynamic (CFD) methods.

In work by Yamamoto and Hill [1], the authors investigated the flow field of a scaled cabin of a pick-up truck, using tuft visualisation and a Reynolds averaged Navier Stokes (RANS) CFD model. Ishihara et al [2] applied a laser flow visualisation method to a scale model of a car interior and compared the results to a RANS CFD model. In work by Aronson et al [3], particle image velocimetry (PIV) was used in a full scale car interior and compared to a CFD model. In a similar experimental and numerical approach by Kataoka et al [4], the flow model results were extended to predict the temperature distribution around the cabin. In this case, the behaviour of the ventilation jets and their effect on the temperature of passengers were investigated. In work on a 50% scale model by Yang et al [5], the car interior flow was also used to characterise the effect of different air conditioning mass flow rates on the cabin flow field. In this case, as in previous examples, a combination of PIV and CFD were used to predict and validate the cabin flow field. A similar example is also found in a bus cabin to test the different ventilation modes and their effect on the flow field [6].

In other examples of vehicle interior flow fields, work has been published on a rail car cabin for fire safety [7] and following the SARS pandemic, work was completed on the distribution of aerosols in aircraft cabins, including the simulation of a passenger coughing [8,9]. Connected to these studies, flow fields in commercial buildings have also been studied [10] and there is significant literature on aerosol dispersion in indoor environments, in buildings and vehicles [11 - 16]. In the case of characterisation of particle dispersion in these environments, a number of different experimental techniques can be used [9,11], ranging from light scattering methods to radioactively doped particles.

In all the cases discussed previously of vehicle interior flow fields, the vehicles were stationary and the effect of the vehicle movement, in terms any longitudinal or lateral acceleration, was not accounted for. This accounts for the fact that there is no previous literature for comparison in Section 3. In the following paper, experimental results of an interior vehicle flow, from an ambulance rear saloon are presented, for both a stationary and a moving vehicle. The results investigate the flow field for both steady and transient motion of the vehicle and the particle dispersion of smoke or helium bubbles, with and without the ceiling air ventilation system, turned on in the saloon. In this work, there is an assumption that saloon air quality, critical to paramedics and patients, is related to particle dispersion rate, which is influenced by the flow field generated from the saloon ventilation systems. The authors believe these are seminal flow and dispersion measurements from a moving vehicle.

## 2. Experimental Methodology

The following section will outline the experimental methodology and set-up in the ambulance and the different techniques used to characterise the flow field and the bulk particle dispersion characteristics, in the vehicle saloon. In all cases the techniques were set-up to allow measurement of data with the vehicle stationary and whilst driving. This presented several challenges, including camera movement during driving and the nature of the confined space in the saloon, which will be discussed further in the paper.

The general experimental approach taken by the authors was to record two separate sets of data which included 1) mapping the flow field from a key measurement plane inside the ambulance and 2) recording the particle dispersion characteristics from a position adjacent to the flow measurement plane. This approach would allow general conclusions to be made about the effect of the flow field on particle dispersion characteristics, under different ventilation and driving conditions. This linkage between particle dispersion rates, the ventilation modes and the driving state of the ambulance was a critical question, that needed to be addressed in the research project. Particle dispersion rates were also assumed to be a robust general measure of the air quality possible inside the saloon, which is a major consideration for paramedics and patients inside the vehicle. More detailed quantitative-based findings between air flow and particle dispersion would require a computational fluid dynamics model, but this data was not available in this project.

As the measurement plane selected in the saloon had significant dimensions (2m x 1.5m), several velocity measurement techniques had to be used in separate measurements, to capture a combination of quantitative velocity data and qualitative flow field patterns. Interpretation of the separate velocity datasets and flow visualisation videos was then completed through observation and comparison, to yield general flow features and flow field characteristics in the saloon. The velocity datasets from the flow visualisation and hot wire anemometer were also compared by using a common set of axes, with an area of overlap in the centre of the measurement plane. The following section will outline these techniques and the ambulance test bed in more detail.

## 2.1. Ambulance Test Bed

A Fiat Ducato ambulance vehicle was loaned to the authors by the U.K. National Health Service (NHS) East Midlands Ambulance Service (EMAS) for the experiments and converted into the flow laboratory. To allow the mounting of the flow visualisation and particle dispersion equipment, the paramedic seat at the front of the saloon was removed and a truss style mounting was bolted onto the seat mounts with a tabletop (Figure 1). Further mounts were also placed onto saloon wall of the ambulance near the side door and the upper storage compartment, to allow mounting of the flow visualisation cameras. Additional equipment, such as the flow visualisation smoke seeder and power supply systems were secured onto the floor, to allow measurements during driving of the vehicle. Furthermore, black out cloths were mounted onto the walls in areas viewed by the visualisation cameras, to reduce light reflection and improve image quality (see Figure 2).

The ambulance was fitted with a ceiling extractor fan or ‘vent fan’, which could be set on a ‘intake’ or a ‘extract’ mode. There were also additional ventilation ducts towards ceiling level at the front of the saloon, termed ‘front vents’. These were only effective during vehicle driving, to supply additional fresh air into the saloon and they were dependent on the vehicle speed and the raised pressure at the front of the vehicle. In any subsequent discussion, the different ventilation modes are referred to, as listed in Table 1.

Vent Fan Mode	Notes
Off	Ceiling fan off, only front vents open
Intake	Ceiling fan on, supplying air from outside into the saloon, front vents open
Extract	Ceiling fan on, removing air from inside the saloon to the outside, front vents open

Table 1 – Ambulance ventilation modes (in all cases front vents open)

## 2.2. Flow Visualisation Methods

Several flow visualisation methods were used to characterise both general and detailed flow patterns. For qualitative interpretation, light sheet visualisation was used and for quantitative visualisation, particle image velocimetry (PIV) [18] data was recorded. In both cases, a common measurement plane was defined by a laser light sheet positioned about the longitudinal stretcher centreline. This plane was chosen to best reflect any potential influence of the flow field on the patient on the stretcher, or adjacent paramedics working in the saloon.

To generate the flow visualisation light sheet, a Coherent DPSS solid state Nd:YAG Genesis laser, with 514nm output and a power of 200mW was directed through a rotating optical hexagon glass element, which scanned the light beam at selected frequencies from several Hz to several hundred Hz. Smoke and helium filled bubbles were used to visualise the flow patterns and record PIV data (see section 2.2.2). The laser sheet could be repositioned at various angles up to 20° from the horizontal, to capture the different imaging areas, including the vent fan area on the ceiling. Blackout cloth was also mounted on the far wall of the ambulance to reduce reflections in the images. A general summary of the imaging configuration, showing the light sheet position, the common flow origin axes and the interior dimensions, is shown in Figure 3.

### 2.2.1. Qualitative Visualisation

For qualitative flow visualisation, a Go-Pro camera, with an image resolution of 640 x 480 pixels, was mounted at several positions towards the rear of the saloon, to record a movie at 30Hz of the whole laser light sheet and saloon area. This viewpoint allowed estimations of bulk flow movement in the corresponding area above the patient and allowed general analysis of the effect of the vent fan on the ceiling of the cabin, or other transient motions in the flow field. Processing of these images for detailed bulk flow estimations are also discussed in more detail in section 2.2.3.

### 2.2.2. Quantitative Visualisation

For detailed quantitative flow visualisation, a particle image velocimetry (PIV) [18] system was used. The PIV system was based on the same laser visualisation light source as the flow visualisation.

The PIV imaging system used two different cameras. For high spatial resolution measurements, a Sony  $\alpha$ 600 with a resolution of 6024 x 4024 pixels was mounted perpendicularly, at several different positions, to observe the light sheet. This set-up observed larger global flow patterns. The cameras were configured for a frame-rate of 10Hz and bursts of 20 images were stored in the camera's memory. Typical sets of 100 images were taken for each acquisition sequence to allow sufficient averaging of the flow field from a given sample. Imaging areas ranged from 600mm x 400mm, up to a maximum of 2000mm x 1500mm. Peak measurable velocities with this system were between 200 - 400 mm/s, depending on the magnification.

The lower resolution camera was a Forward Looking Infrared (FLIR) Blackfly S BFS-PGE-50S5C-C CCDs with a resolution of 2448 x 2048 pixels and a frame rate of 22 Hz. These cameras were positioned on the rail opposite the stretcher and allowed smaller 'zoomed' in areas of 250mm x 200mm, to look at more local flow structures. Peak measurable velocities were similar to the high resolution PIV system.

The seeding system was initially based on mineral oil smoke seeder and prior to PIV acquisition, the seeder was turned on for around 1 minute and then left for a further minute to allow any transients from the seeder heater to damp out and to allow the smoke seeding to distribute more evenly around the interior. The particle size generated by oil smoke seeder, was estimated to be  $1\mu\text{m}$  from the particle dispersion measurements, ensuring a low settling velocity of less than 100mm per hour, ensuring no particle lag when tracking the air flow [17]. This particle size is also consistent with human produced aerosols (see section 2.4). Following a recording sequence, the smoke would then be removed by turning off the laser and ventilating the whole saloon volume by use of the vent fan on extract. This ensured more contrast in the PIV images.

A second LaVision Helium bubble seeder was also employed to seed the flow and improve the particle image quality. This was because the smoke seeding density was found to be difficult to control and typically would over-seed the volume, resulting in the requirement to process the sets of images using larger interrogation regions, discussed in the next section. Use of the Helium bubble seeder also allowed high quality flow visualisation images to be generated by the adding together 7 – 8 image sets, to give quantitative flow visualisation. An example of the different flow visualisation and PIV images is shown in Figure 4.

### 2.2.3. Data Processing Methods

Following acquisition of data from the PIV cameras, the higher resolution image sequences, such as the Sony  $\alpha 600$  image sequences, were converted into 24-bit bitmap bmp images and then 8-bit \*.bmp greyscale format, using the Matlab Image Processing Toolbox. The 8-bit PIV images were uploaded onto a high performance computer for processing using an in-house PIV processing software 'xpiv', as described in [19]. Sequences of 20 images were processed using a cross-correlation averaging routine [20] to improve the signal-to-noise on the images. The PIV data yielded an average two-dimensional vector map of the flow, in the image plane. Typical interrogation region sizes with images from the Helium Bubble seeder were set to 128 x 128 pixels, with 1500 vectors per dataset, corresponding to a spatial resolution of around 18mm per point.

With the PIV images from the smoke seeding, the interrogation region size for the higher resolution images was increased to 512 x 512 pixels, to allow the correlation to be based on smoke generated patterns, rather than particle images. This non-standard approach allowed effective processing over a wide range of smoke densities and was most effective at the early stages of smoke dispersion, when the local smoke patterns were well defined. In this case, spatial resolution reduced to around 30mm and around 1000 vectors per image. In all cases, the raw output velocity data was subsequently filtered using an *a-priori* range and smoothed using a 3 x 3 Gaussian kernel smoothing window, to remove data noise.

The lower resolution GoPro images were also processed using the same methods as described previously. This data would allow more general quantitative analysis of bulk movements of the flow in the saloon. However, in this case, due to the highly defined shape of the light sheet in the images and the background (see Figure 4a), an image mask was applied to isolate the data from the light sheet area, during conversion of the images (Figure 5). This mask was then applied to a sequence of 700 images which were processed with an interrogation region mask of 32 x 32 pixels to yield 800 vectors with an average resolution of 40mm. A monitor point was then selected from the vector maps to track bulk movement of the flow. These results will be discussed in section 3.

### 2.3. Hot Wire Anemometry Measurements

To supplement the flow visualisation and PIV measurements, a hand-held hot wire anemometer (HWA), model Solomat MPM500e, was positioned at 40 points around the same PIV measurement plane and a series of single, horizontal u component, mean velocity measurements were made, through a range of fan extraction and driving conditions. The measurement points and data are shown in Figure 6. These data were used for comparison with quantitative PIV data from the flow visualisation and for overall interpretation of the saloon flow patterns. They also allowed measurements of higher peak velocities near the ceiling vent fan, where velocities exceeded 1 m/s under some test conditions and which were outside the PIV dynamic range. The stated resolution of the HWA unit was 0.01 m/s with a peak measurement range up to 15 m/s. However, measurements were recorded when the velocity on the unit display was stable to within +/-0.1 m/s, at each measurement point.

### 2.4. Particle Dispersion Measurements

To quantify the effect of the ambulance saloon ventilation and flow field on the particle dispersion, a further set of measurements were taken using the smoke seeding and a GRIMM optical particle counter. The general principle of these measurements was to monitor the particle decay in the saloon under different driving and fan extraction conditions and qualitatively relate this effect to the flow field observations. The mean particle size of the smoke was known to be under 1 $\mu$ m and therefore would be consistent with the size of any neutrally buoyant aerosol that may disperse inside an ambulance from a patient [21]. Given an initial condition, by monitoring the dispersion rate of the particles, it was expected this could give estimates of gross effects of the flow field ventilation system, on the improvement of cabin air quality.

For all measurements, the counter was set-up to sample a particle size range of 0.25 $\mu$ m – 32 $\mu$ m, every six seconds, with a flow rate of 1.2 litres per minute. In these measurements, with the ambulance saloon clear of any visible smoke, a background count was taken using the GRIMM and an initial injection of smoke for was made 30 seconds in the cabin. The smoke was then left to disperse around the cabin for two minutes, before measurements began. The particle count was then monitored and the dispersion rate analysed. In all cases, to ensure a consistent comparison of datasets, all tests were normalised to 2000 /cm<sup>3</sup> for a time series decay.

A typical dispersion profile is shown in Figure 7, where the dispersion sequence is separated into a 'natural' decay rate and a 'treatment' decay rate, with the latter defined at a specific particle count level in the measurement sequence. The initial injection sequence is also visible at the beginning of the data sample. The 'treatment' decay rate is then analysed with respect to an exponential decay with a particle count  $y$  and constant  $a$ :

$$y = ae^{bx} \quad \text{Eqn (1)}$$

such that the decay rate of interest is defined through the exponent constant  $b$ , using best fit curve statistics for each portion of the time sequences. A summary of the different dispersion rates is shown in Figure 8 and will be discussed in the next section.

### 2.5. Laboratory Environment and Challenges

Several challenges needed to be overcome due to the unusual environment of the ambulance laboratory, particularly with the vehicle in motion.

One of the key challenges of the PIV set-up was vibration of the camera mounts and movement of the laser sheet, during vehicle motion. A continuous laser sheet was found to be more susceptible to vibration, as the particle images would streak due to the long exposure times required for particle exposures, with the low and high resolution cameras. This problem was reduced by using a scanning laser sheet system, which both increased the effective laser power of a given particle exposure, but also allowed for larger imaging areas. A pulsed laser would have provided a greater increase in power, but the health and safety considerations were thought to be unacceptable, given where the vehicle was driven and operated.

Camera mount vibration was also reduced, by using cross braces on the mounts and securing the camera mounts off rigid structures such as seat bases. Furthermore, any auxiliary equipment was mounted on the floor and braced onto firm structures such as cupboard frameworks. Space was limited too and so positioning of equipment in the saloon needed care planning before any operation.

Further considerations in the PIV set-up were live and remote viewing of the camera view and remote triggering of the cameras. In the first case, HDMI cable extensions permitted a live camera monitor in the saloon or driver's cabin and an extended length of shutter cable, with an electronic shutter, was adapted for triggering the high resolution camera remotely. Remote operation of the camera not only reduced operator induced vibration when triggering, but also allowed operation from the driver cabin where necessary. This flexibility of the set-up also provided more options, when different seeding material and seeding densities were being tested in the saloon.

### **3. Results and Discussion**

The following section outlines the results from the flow visualisation and particle dispersion measurements and then discusses the general flow patterns and particle dispersion characteristics under the different vehicle driving conditions and saloon extraction settings. Velocity and flow visualisation datasets use a common origin and axes set to aid any interpretation of the overall flow field patterns.

#### **3.1 Static and Steady Driving Flow Visualisation**

The steady state flow patterns established in the cabin were interpreted by analysing a combination of the HWA and PIV data. In general, when comparing data from both measurement systems, overall velocity magnitudes were comparable at equivalent positions in the flow plane, and the flow field patterns were consistent with both measurement sets, in any areas of data overlap. General flow patterns observed in the flow visualisation were also similar to the quantitative data. Furthermore, during steady driving conditions up to 60 mph or whilst the vehicle was stationary, the general flow field patterns, for a given vent fan condition, did not appear to significantly change. This indicated a minimal effect of the front vents on the flow fields.

The most significant changes in the gross flow fields and patterns were found with the vent fan on extract or intake mode. To illustrate this, Figure 9a and Figure 9b shows PIV data taken using the He bubble seeding under a vent off and vent extract condition. Here the change in the flow field from the quiescent vent off condition to vent extract condition is clear and supported by the flow statistics of Figure 9c, where the mean flow velocity increases from 27mm/s to 52mm/s when the vent fan is selected to extract. The other effect of the vent extract is to move the bulk flow away from the patient area, which would be critical in

improving the air quality around the patient. Therefore not only does the extract function increase the bulk flow velocities, it also ensures a preferable flow direction over the patient. In this case, the HWA data in vent extract mode generally matched the data recorded using the PIV method, at corresponding points in the flow field.

Evidence of the effectiveness of the ceiling vent system for cabin ventilation was also found from the HWA data. Figure 6 shows the general  $u$  component flow field magnitudes for the vent extract and vent intake modes. It can be seen that the vent intake mode provides significantly higher velocities near the ceiling, increasing the flow speed near the vent outlet from around 300mm/s in extract mode, to 1000mm/s or higher in intake mode. The intake mode also reverses the flow direction near the ceiling when compared to extract. This additional flow speed is highly localised near the ceiling vent, as 200mm from the vent area, the bulk flow velocities have reduced to 100mm/s – 300mm/s in intake mode. This matches velocity magnitudes in extract mode. However, as will be discussed in section 3.3, the reverse in flow direction to intake rather than extract, has a major effect on the flow patterns around the saloon, but less effect on the particle dispersion rates.

The variation in particle dispersion rates, both with different driving and vent conditions is highlighted in Figure 8, where it can be seen, that under static vehicle or constant speed driving conditions, there is little variation in the particle decay rates in the saloon. There is a slight improvement in the decay rates when the fan is set to extract rather than intake, in static driving conditions. But this variation is within the standard deviation of the natural decay rates and may also be connected to the vent configuration on the ambulance roof. Here local flow patterns around the ceiling vent area may be more affected in extract mode whilst static, than when the vehicle is driving as the vent on the vehicle roof is influenced by variations of dynamic pressure. However, it is clear that ventilation effectiveness in the saloon, consistent with the higher particle decay rates, will be achieved in either extract or intake modes and this reinforces the findings of the PIV and HWA data.

### **3.2. Dynamic Driving Flow Visualisation**

The experimental set-up allowed recording of flow visualisation and PIV data throughout the driving measurement session, from vehicle start to shut down. During initial measurements inside the vehicle, basic observations of the GoPro video appeared to show significant movement of the bulk flow when under dynamic driving conditions, independent of the extract or intake vent settings. Therefore a sequence of GoPro images was processed using the xpiv software, to analyse the flow movement in the saloon. Samples of these PIV vector maps are shown in Figure 10a and Figure 10b. It should be noted that the scaling is not linear due to the GoPro viewing angle. The results are taken at known times in the video sequence where the bulk flow was observed to have changed direction. This effect is confirmed in the vector maps, where the flow is moving away from the front of the saloon at  $t = 5.0$ s and then reverses towards the front of the saloon by  $t = 11.3$ s. In this particular time sequence, the vehicle was accelerating from less than 10mph to approximately 30mph and then braking again to less than 10mph.

To further quantify this bulk movement, a sample point was selected in the centre of the vector fields, at  $x = 1450$ mm,  $y = 580$ mm, and the  $u$  component of velocity plotted for the full image sequence of 700 samples, as shown in Figure 10c. The plot shows a clear change in direction of the bulk fluid flow at around  $t = 6.5$  seconds, with further evidence of a shift in flow direction at  $t = 15$ s. The bulk change is in the order of 200mm/s and originates from an inertial difference, imparted on all the saloon fluid during the vehicle braking or acceleration. This fluid inertial change thus exceeds the steady state fluid inertias in the flow field, when the vehicle was initially driving at constant speed. This is consistent with the dominant range



of velocities in the steady condition, which are of the order of 100mm/s in the flow field. Therefore with a change in the vehicle velocity in excess of this, the momentum change of the fluid bulk must generate a force in excess of these local fluid inertias, resulting in these bulk flow reversals, as seen in the data.

This finding has significant consequences for the fluid mixing and aerosol dispersion in the vehicle and may enhance mixing or aerosol dispersion, as shown in the results in Figure 8. However, this flow movement may also degrade the effectiveness of the vent induced flow field, to remove aerosols from the patient area, for example on extract. It is unlikely a higher power extraction system would be able to overcome the bulk fluid motions generated through fluid inertia changes, under these dynamic driving conditions. Hence, to retain a consistent removal of aerosol from the patient area under dynamic driving conditions, a more localised extract system may be required.

### **3.3. General Flow Pattern Interpretation**

Given the different sources of flow field data and the GoPro flow visualisation videos, it is possible to construct a general interpretation of the expected flow field pattern patterns, under static or constant driving conditions. Based on the patient centreline plane, Figure 11a and Figure 11b show the predicted flow patterns for the extract and intake vent modes.

If we consider the extract flow field, it is thought to be dominated by a large recirculation zone, which is primarily driven by a ceiling jet convecting towards the vent and reinforced by flow from the front vent. There may be a slight reinforcement of this flow by the front vent under driving conditions, but none of the particle dispersion or flow field data had evidence of this. Flow speeds in this primary zone peaked at around 300mm/s nearer the ceiling, reducing to less than 50mm/s in the region of the patient. Flow visualisation data from the rear area of the saloon also suggested the existence of much smaller recirculation and dead zones, which is consistent with expected flow topology and continuity patterns.

If we consider the intake flow field, this field is dominated by a much higher speed ceiling jet, up to 1400mm/s in the vent region, but more typically around 1000mm/s towards the front side of the saloon. This ceiling jet pattern is thought to generate two primary recirculation zones in each half of the saloon which converge up towards the vertical centreline of the vent. This flow was found to be highly turbulent in areas nearer the ceiling and in some cases only HWA data could be measured in these regions, as the level of turbulence prohibited measurement using PIV using the smoke or He bubbles. Given the inertial strength of the ceiling jet, flow visualisation did not indicate any substantial influence of the front vents on these gross flow patterns, with no known dead zones, although it is thought a smaller secondary circulation zone existed towards the rear of the saloon. However, away from the ceiling jets, where the main recirculation zone velocities were less than 100mm/s, the effects of the dynamic vehicle driving were still found to disrupt the primary recirculation patterns, as with the extract mode.

In terms of particle dispersion, it is thought in this intake mode, the particles are removed through the peripheral ventilation vents or door gaps, around the saloon structure, with significant levels of turbulence, dispersing the particles throughout the saloon. This contrasts to the extract mode, where the vast majority of the particles are removed through the ceiling vent with a less turbulent flow field.

## 4. Conclusions

This work has presented what is thought to be seminal flow field and particle dispersion data from an NHS ambulance, under static and dynamic driving conditions and different ventilation modes. The particle dispersion data was based on particle characteristics that are similar to those generated by patients in the ambulance. The work was completed as part of a UK COVID19 Pandemic Preparedness program and used a standard NHS ambulance as a flow visualisation laboratory.

Results from the flow visualisation and PIV data, in a plane positioned above a potential patient, indicated a significant influence of the ceiling fan ventilation system on gross flow field behaviour, inside the ambulance saloon. With the ventilation fan on extract or intake, flow velocities were found to double from a quiescent condition, to around 50mm/s – 100mm/s, moving the flow away from the patient area. The particle dispersion data also showed dispersion decay rates over five times faster when using the ceiling fan in either intake or extract mode. These results were found to be consistent whether the vehicle was stationary or driving at a constant speed of 60mph.

Flow visualisation and HWA data also indicated gross flow patterns were also expected to be influenced by use of extract or intake mode, with significant changes in the recirculation zone patterns under the two modes. Further, the most turbulent flow was found to exist in the intake mode where the highest speed ceiling jets were generated.

Further flow visualisation data with the vehicle under dynamic driving conditions, such as acceleration or braking, was found to substantially disrupt the steady state flow patterns in the saloon, with bulk movement of the flow in the direction of the acceleration or braking action. This was attributed to the inertial effect on the bulk fluid originating from the braking or accelerating force. Under these conditions, the magnitude of the net velocity change on the fluid exceeded any effect generated from the ceiling ventilation system and this effect would be expected to happen under cornering and any other dynamic driving conditions. This result would indicate enhanced local ventilation may be required in the vehicle to prevent disruption of patient ventilation under all driving conditions. Therefore, a key question raised by this work was whether different ventilation modes and driving conditions affect the dispersion rates in the vehicle and the results show this to be the case. Hence, these findings may influence future operation of the ventilation systems and future saloon design.

## Acknowledgements

The authors would like to acknowledge the support of the Royal Academy of Engineering under Pandemic Preparedness grant number EXPP2021/1/194. The authors would also like to acknowledge the input of Dr Adam Boies from Cambridge University and the company Q-Flo Limited for use of their prototype nanotube filter. Jamie Trembath from FAAM kindly loaned the GRIMM OPC and the ambulance used was provided by the South Central Ambulance Service NHS Foundation Trust via Phil Pimlott.

## References

1. Yamamoto, K. and Hill, W., "Interior Flow Visualization of a Small Pick-Up Truck and A/C Feeling Estimate", *SAE Technical Paper* 900082 (1990)

2. Ishihara, Y., Hara, J., Sakamoto, H., Kamemoto, K. et al., "Determination of Flow Velocity Distribution in a Vehicle Interior Using a Visualization and Computation Techniques", *SAE Technical Paper* 910310 (1991)
3. Aronson, D., Chroner, Z., Elofsson, P., and Fellbom, H., "Comparison Between CFD and PIV Measurements in a Passenger Compartment", *SAE Technical Paper* 2000-01-0977 (2000)
4. Kataoka, T. and Nakamura, Y., "Prediction of Thermal Sensation Based on Simulation of Temperature Distribution in a Vehicle Cabin", *Heat Transfer Asian Research*, 30 (3), p195 - 212 (2001)
5. Yang, J.H., Kato, S. and Nagano, H., "Measurement of Airflow of Air-Conditioning in a Car with PIV", *Journal of Visualization* 12(2), 119-130 (2009)
6. Hossam, M., Fouad, M., and Abou-Zaid, A., "Numerical Investigation of Airflow Patterns and Thermal Comfort in a Bus Cabin", *SAE International Journal of Passenger Cars - Mechanical Systems* 13(2), 145-156 (2020)
7. Craig, M. and Asim, T., "Numerical Investigations on the Propagation of Fire in a Railway Carriage", *Energies* 13, 4999; doi:10.3390/en13194999 (2020)
8. Isukapalli S.S., Mazumdar S., George P., Wei B., Jones B., Weisel C.P., "Computational fluid dynamics modeling of transport and deposition of pesticides in an aircraft cabin", *Atmos. Environ.* 68, 198 – 207 (2013)
9. Sze To G.N., Wan M.P., Chao C.Y.H., Fang L. & Melikov A., "Experimental Study of Dispersion and Deposition of Expiratory Aerosols in Aircraft Cabins and Impact on Infectious Disease Transmission", *Aerosol Science and Technology* 43, p466–485 (2009)
10. Calautit, J.K., Hughes, B.R., "Measurement and prediction of the indoor airflow in a room ventilated with a commercial wind tower", *Energy and Buildings* 84, 367–377, (2014)
11. Byrne, M.A., Goddard, A.J.H., Lange C. and Roed, J., "Stable tracer aerosol deposition measurements in a test chamber", *J. Aerosol Sci.*, 26, 645–653 (1995)
12. Batterman, S., Jia, C., Hatzivasilis, G. and Godwin, C. "Simultaneous measurement of ventilation using tracer gas techniques and VOC concentrations in homes, garages and vehicles", *Journal of Environmental Monitoring* 8, 249-256 (2006)
13. Holmberg, S., Chen, Q., "Air flow and particle control with different ventilation systems in a classroom", *Indoor Air* 13, 200-204 (2003)
14. Chen, F., Yu, S.C.M., Lai, A.C.K., "Modeling particle distribution and deposition in indoor environments with a new drift-flux model", *Atmospheric environment*, Vol. 40, p. 357-367 (2006)
15. Zhang, Z., Chen, Q.. "Experimental measurements and numerical simulations of particle transport and distribution in ventilated rooms", *Atmospheric Environment* 40(18), p. 3396-3408 (2006)
16. Zhao, B., Yang, C., Yang, X. and Liu, S., "Particle dispersion and deposition in ventilated rooms: testing and evaluation of different Eulerian and Lagrangian models", *Building and Environment* 43(4), 388-397 (2008)
17. Melling A., "Tracer particles and seeding for particle image velocimetry", *Meas. Sci. Technol.* 8, 1406-1416 (1997)
18. Raffel, M., Willert, C.E, Scarano, F., Kähler, C.J., Wereley S.T., Kompenhans J., "Particle Image Velocimetry: A Practical Guide – 3<sup>rd</sup> Edition", *Springer International Publishing* (2018)
19. Lawson, N.J. and Davidson, M.R., "Self-sustained oscillation of a submerged jet in a thin rectangular cavity", *Journal of Fluids and Structures* 15(1), pp59-81 (2001)

20. Hart, D.P., "PIV Error Correction", *Exp. In Fluids* 29, p13-22 (2000)
21. Johnson G.R., Morawska L., Ristovski Z.D., Hargreaves M., Mengersen K., Chao C.Y.H., Wan M.P., Li Y., Xie X., Katoshevski D., Corbett S., "Modality of human expired aerosol size distributions", *J. Aerosol Sci.*, 42, 839–851 (2011)

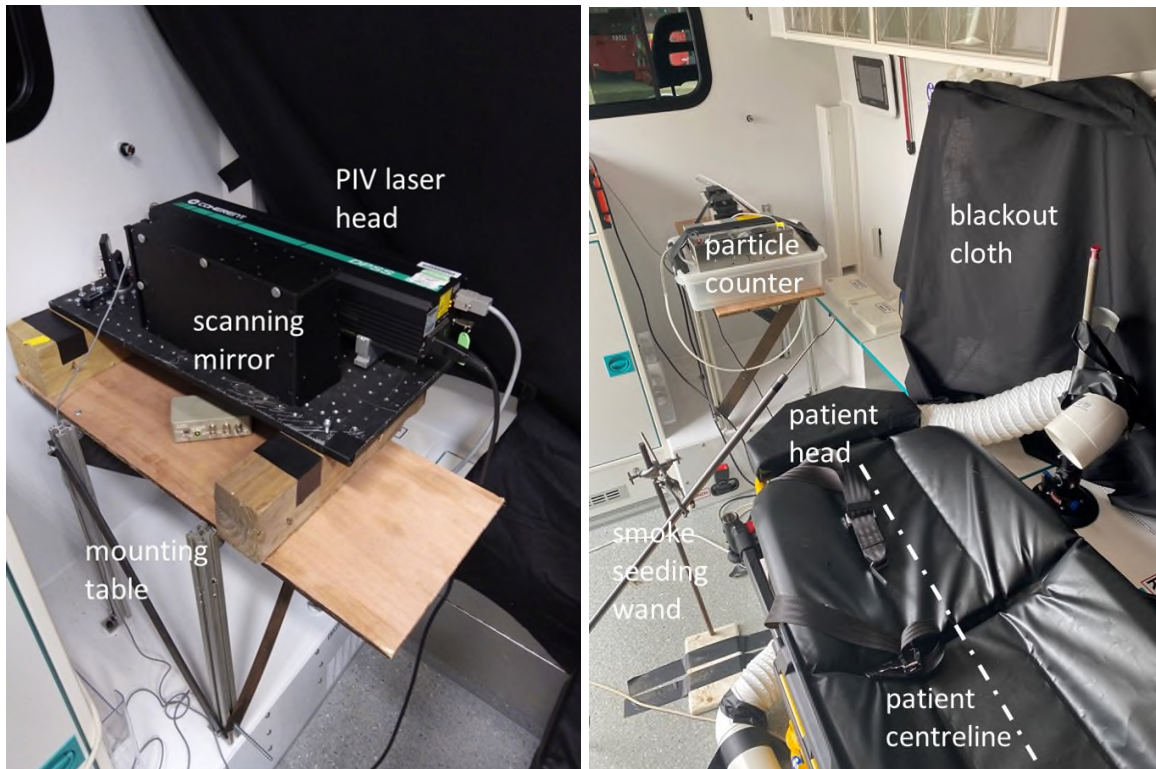


Figure 1 – Mounting system with flow visualisation laser and particle counter



Figure 2 – General layout of lab equipment in ambulance

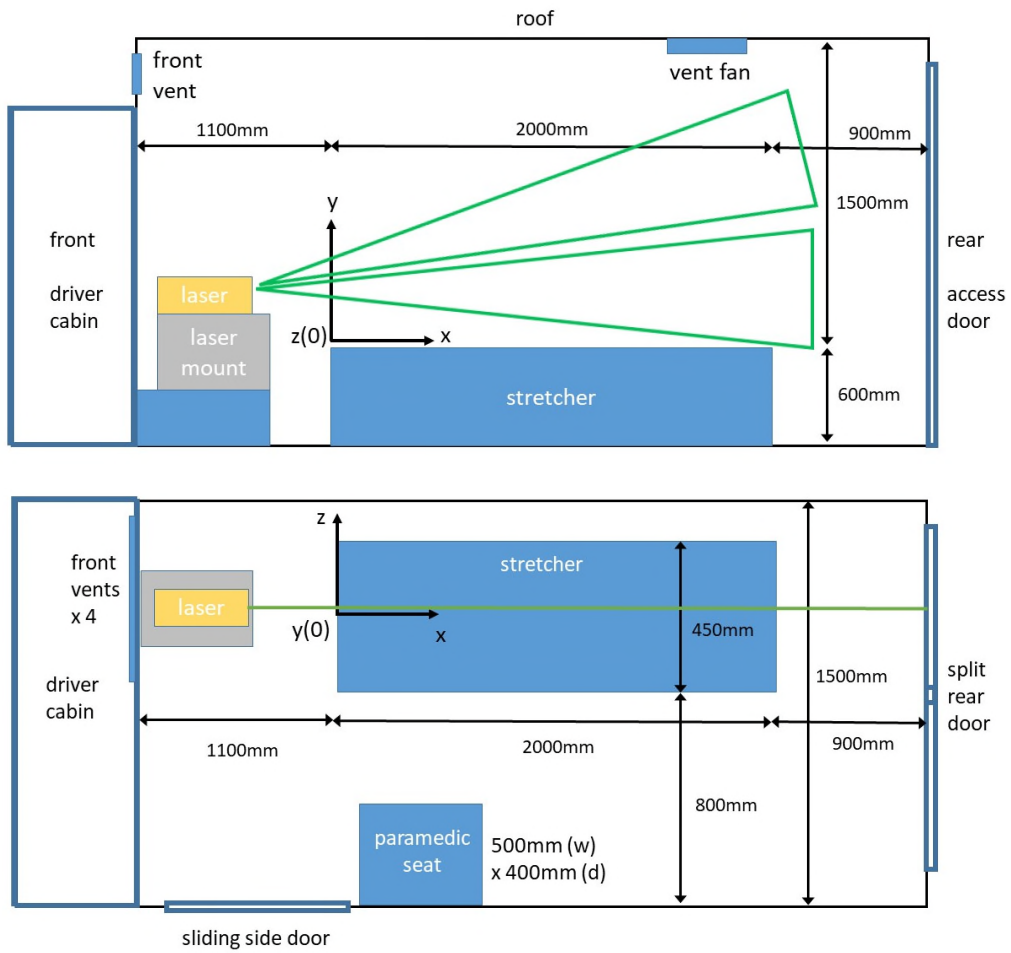


Figure 3 – Laser light sheet flow measurement set-up and axes (side view and plan view)



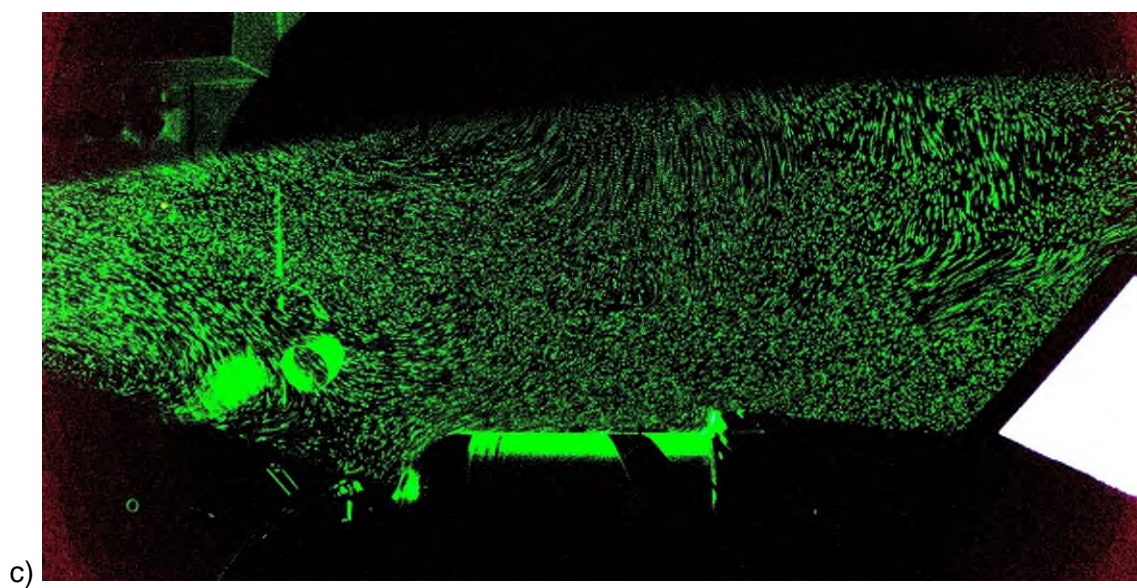
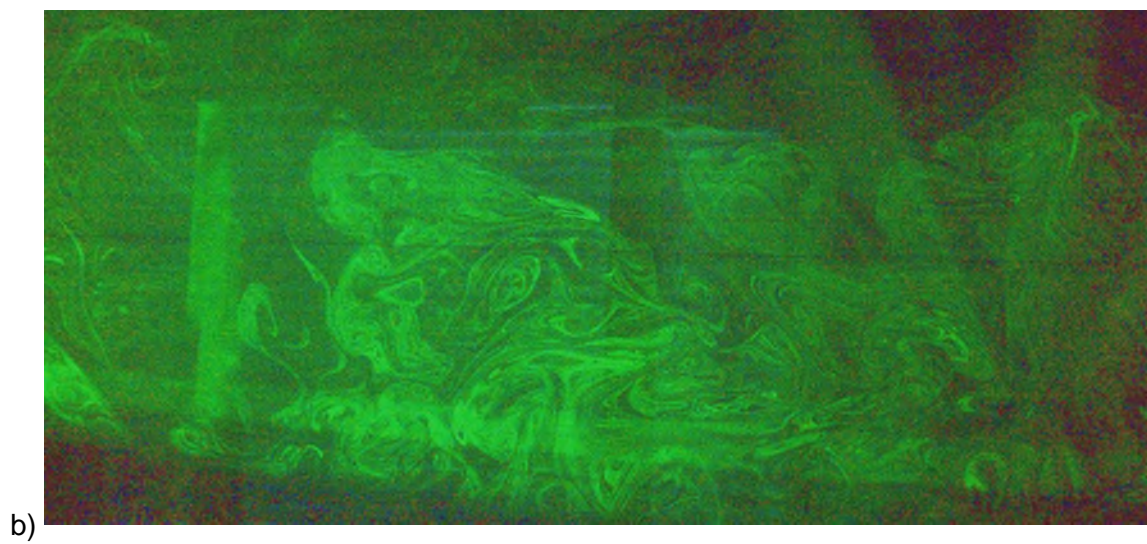


Figure 4 – An example of the flow visualisation PIV images using a) the smoke generator and GoPro b) the smoke generator and Sony  $\alpha$ 600 c) the Helium bubble seeder and Sony  $\alpha$ 600

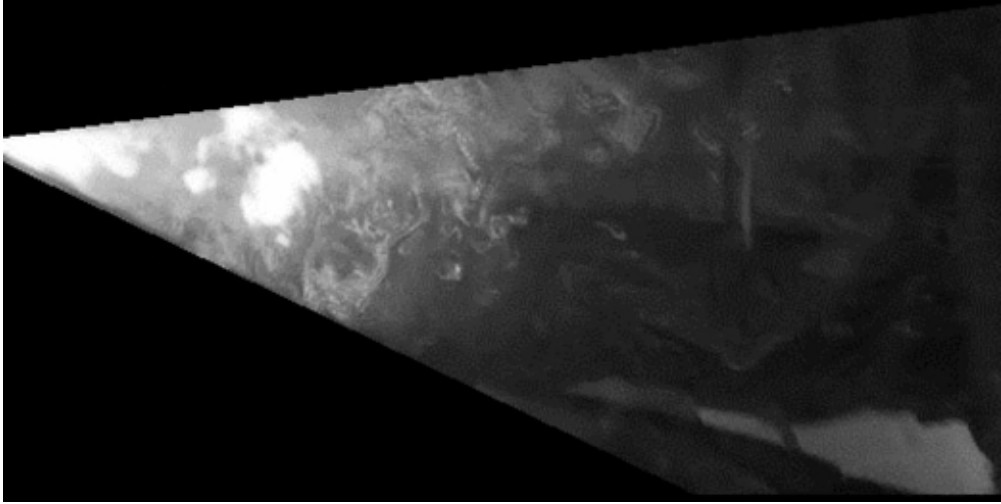
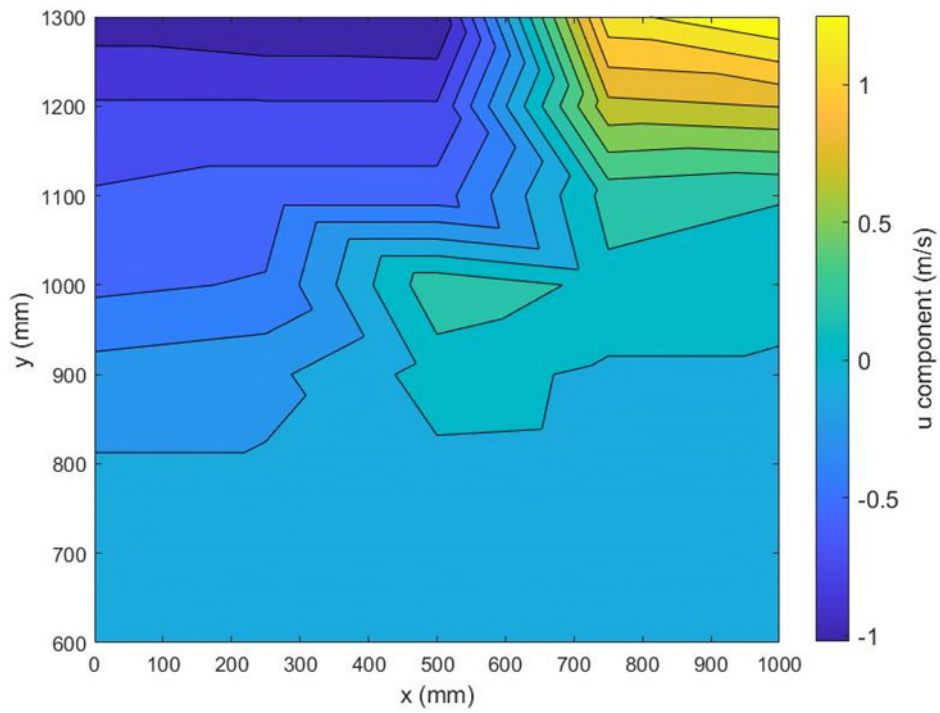
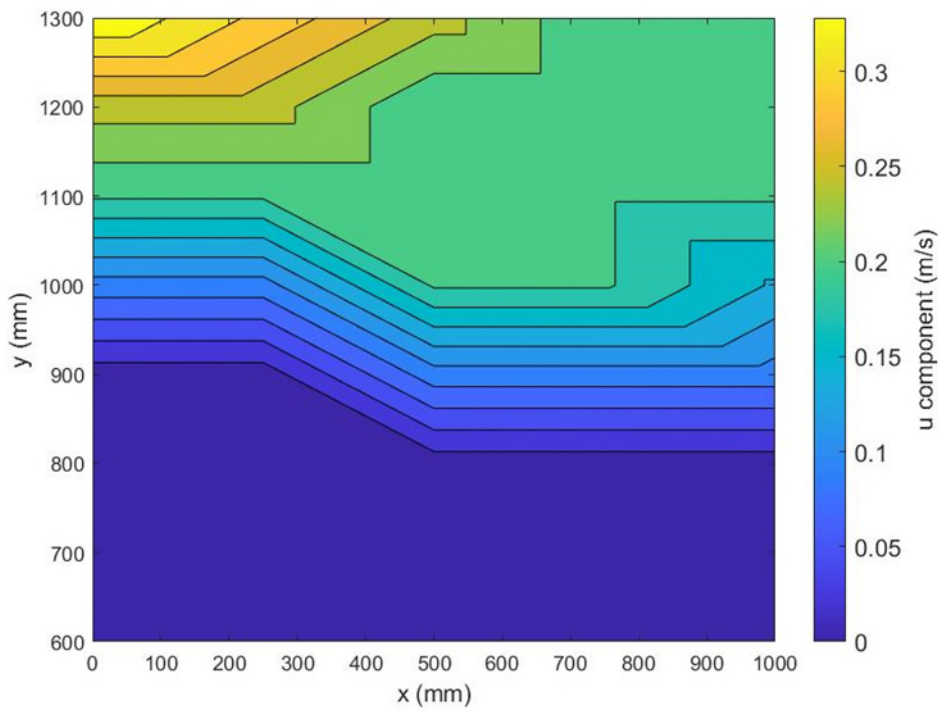


Figure 5 – An example of an 8 bit GoPro flow visualization image with the light sheet image mask **for processing with the xpiv bespoke software**





a)



b)

Figure 6 – Hot Wire Anemometry (HWA) data about the patient centreline a) vent fan intake b) vent fan extract

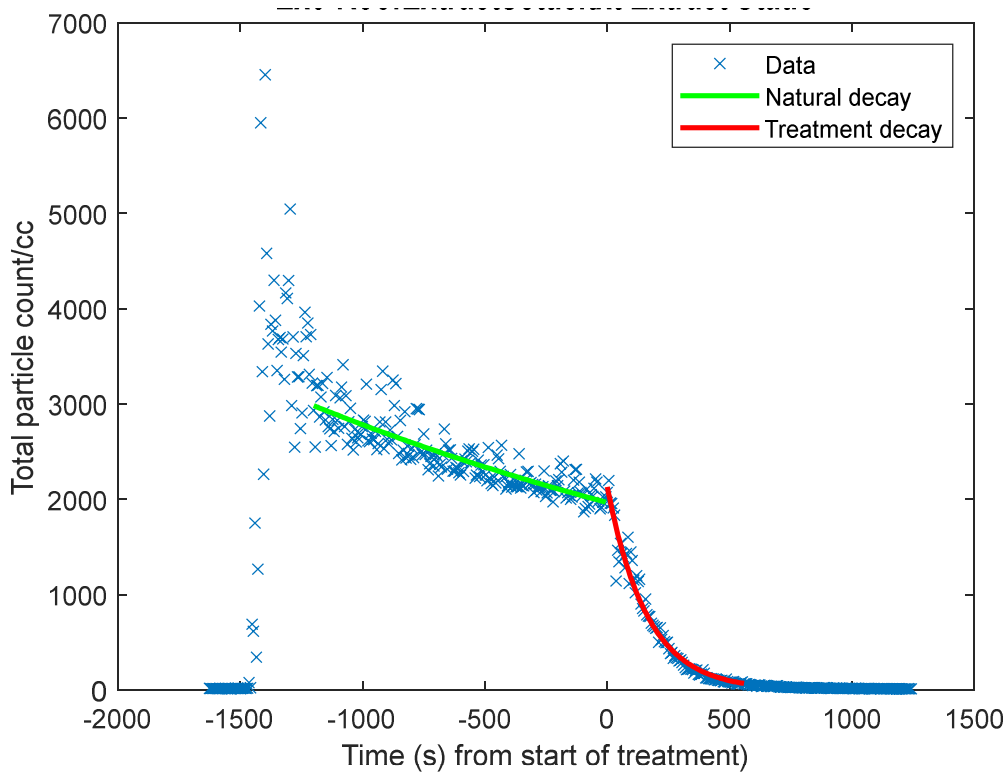


**Figure 7 – A typical particle decay sequence taken using the GRIMM particle counter, following an initial injection of smoke in the saloon**

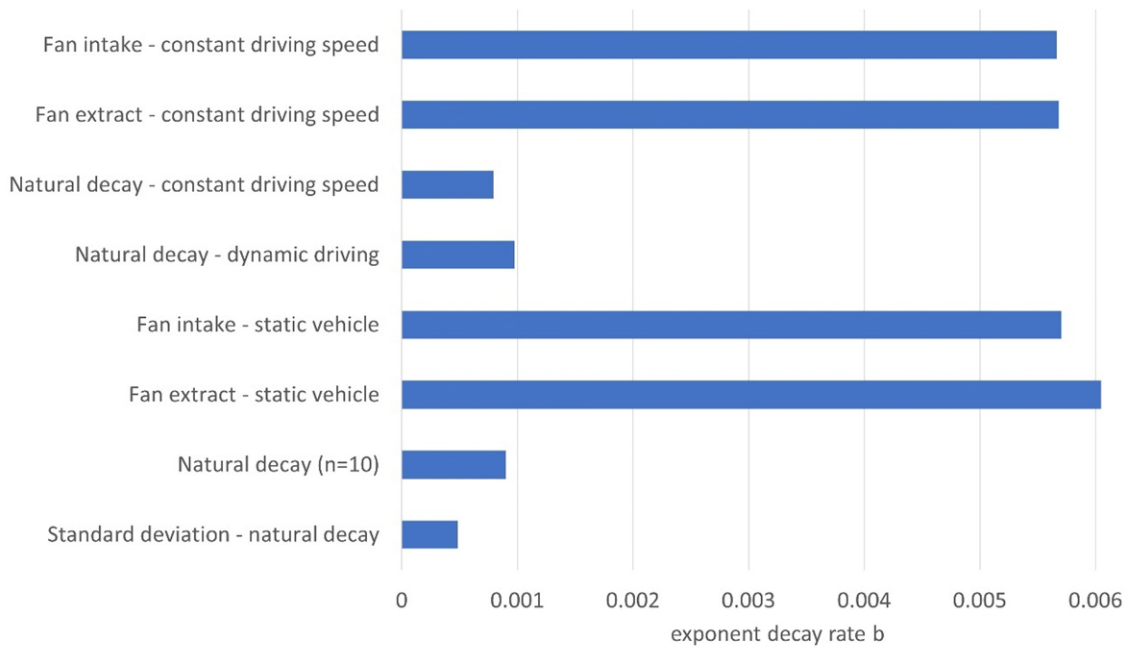


**Figure 8 – Summary of aerosol dispersal characteristics under several driving conditions**

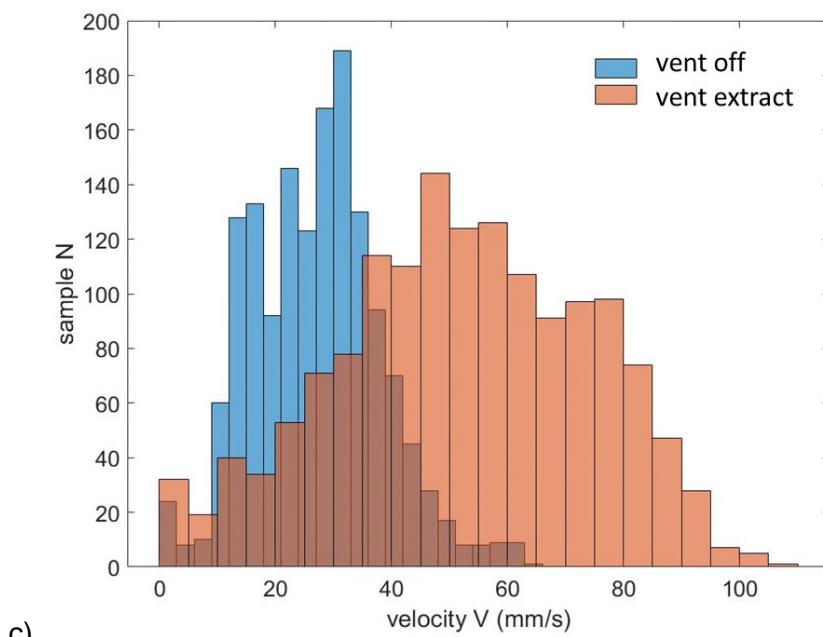
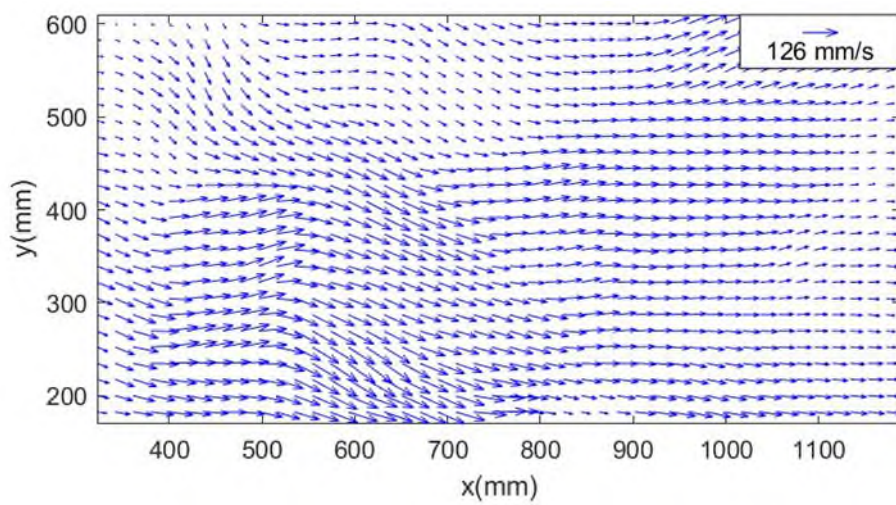
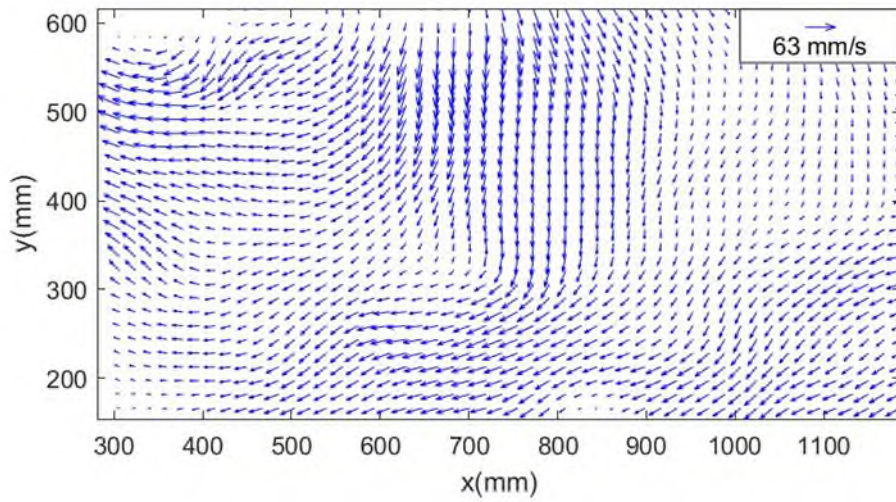
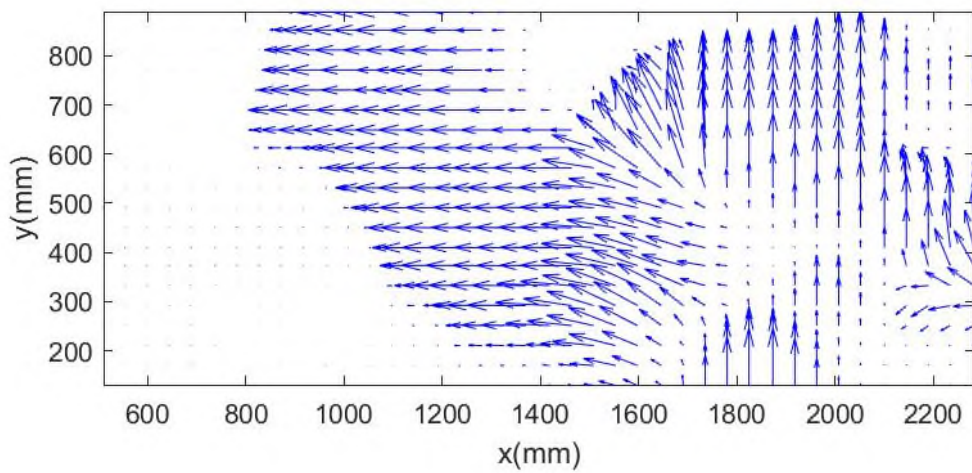
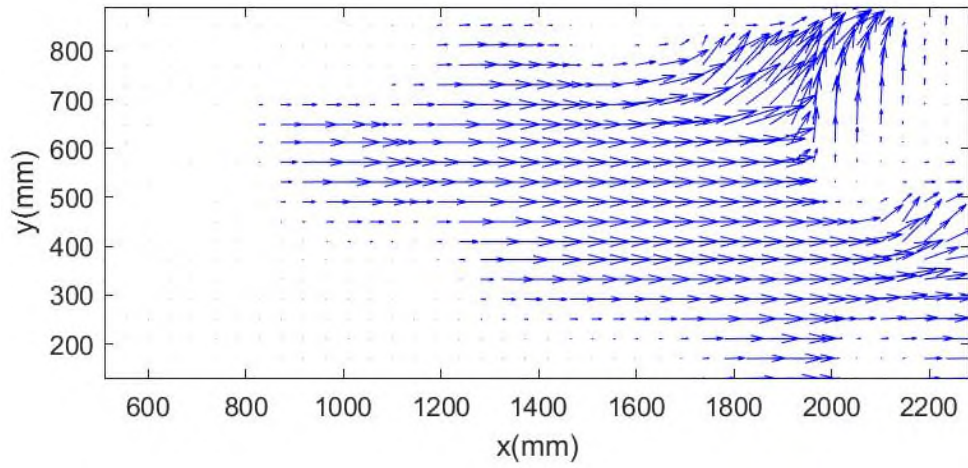
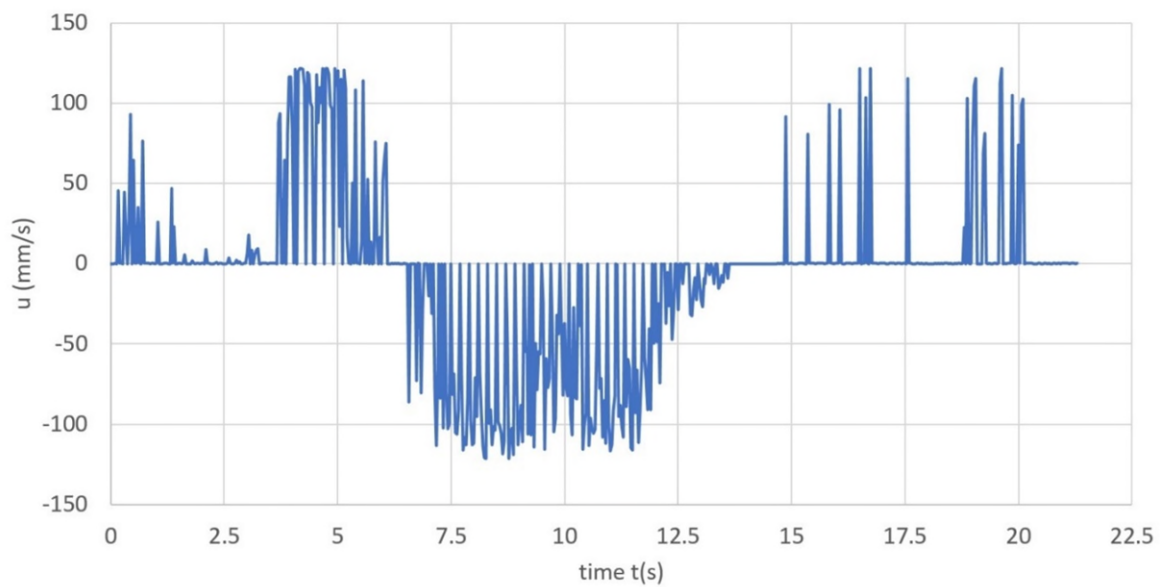


Figure 9 – PIV data a) vent fan off b) vent fan extract c) velocity magnitude histogram. (note: in a) and b) 63 mm/s and 126 mm/s are velocity vector scales and the distances x and y are referenced to the stretcher origin shown in Figure 3)

a)



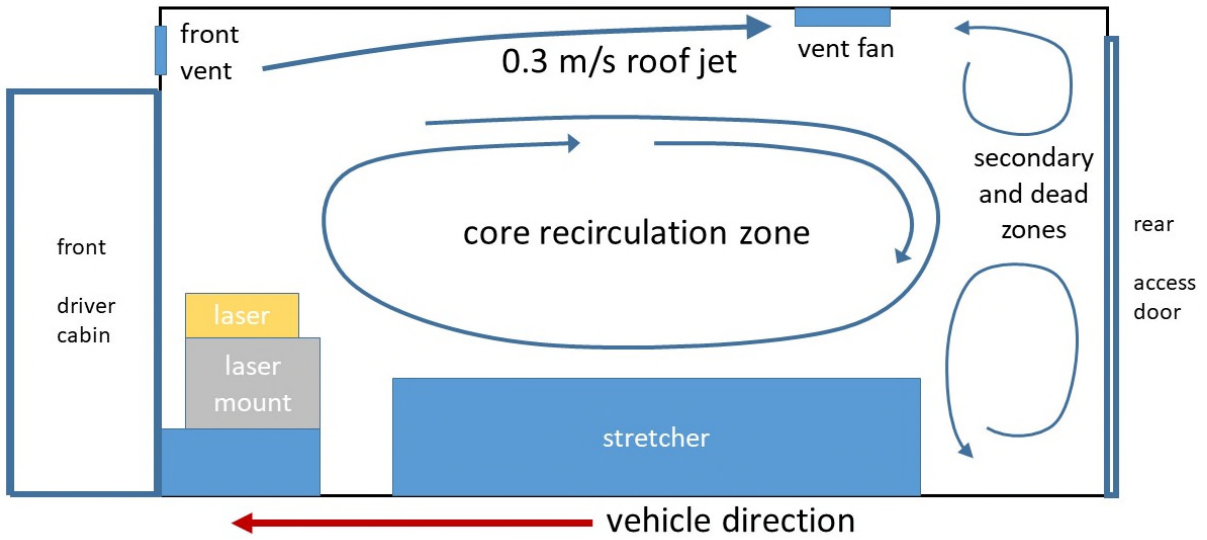
b)



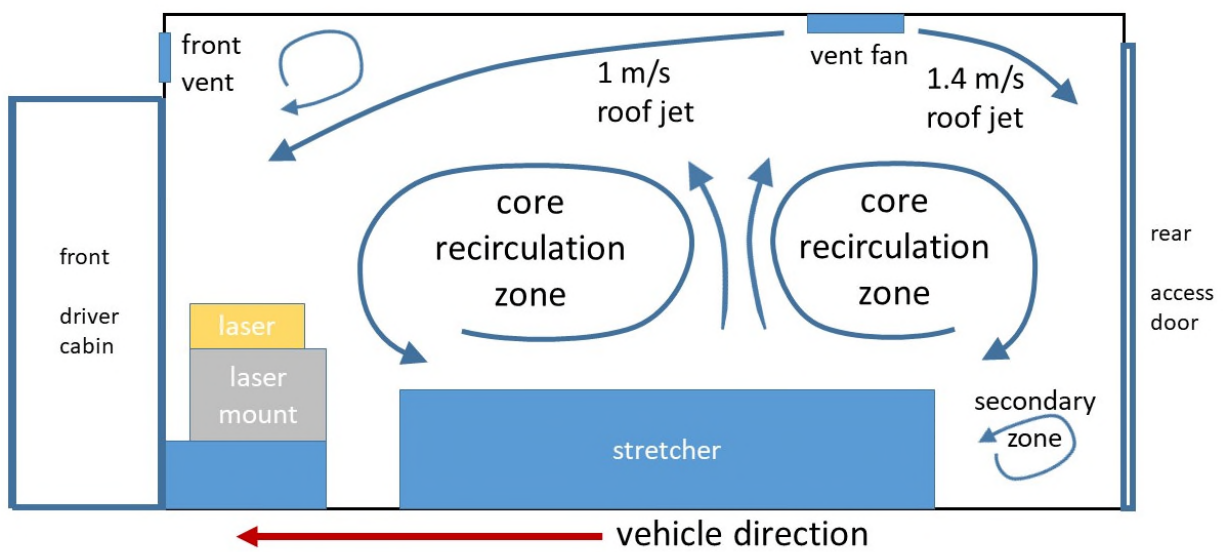
c)

**Figure 10 – GoPro Transient PIV data for bulk velocity estimation – vent fan extract a) 5.0s b) 11.3s c)  $u$  sample point ( $x = 1450\text{mm}$ ,  $y = 580\text{mm}$ )**





a)



b)

Figure 11 – Summary of vehicle saloon steady flow pattern interpretations under static and driving conditions a) fan extract b) fan intake

2022-04-07

# Flow visualization and particle dispersion measurements inside an ambulance rear saloon while stationary and in motion

Lawson, Nicholas J.

SAE International

---

Lawson NJ, Blackburn K, Sherwood G, et al., (2022) Flow visualization and particle dispersion measurements inside an ambulance rear saloon while stationary and in motion, SAE International Journal of Commercial Vehicles, Volume 15, Issue 4, April 2022, Article number 23 <https://doi.org/10.4271/02-15-04-0023>

*Downloaded from Cranfield Library Services E-Repository*